Bull. Mater. Sci., Vol. 39, No. 5, September 2016, pp. 1279–1284. © Indian Academy of Sciences.
DOI 10.1007/s12034-016-1254-3

Structural, electrical and electrochemical studies of $LiNi_{0.4}M_{0.1}Mn_{1.5}O_4$ (M = Co, Mg) solid solutions for lithium ion battery

G P NAYAKA[1], K V PAI[1], J MANJANNA[2,*], K C ANJANEYA[1], P PERIASAMY[3] and V S TRIPATHI[4]

[1]Department of Industrial Chemistry, Kuvempu University, Shankaraghatta 577 451, India
[2]Department of Chemistry, Rani Channamma University, Belagavi 591 156, India
[3]Central Electrochemical Research Institute, Karaikudi 630 006, India
[4]Chemistry Group, Bhabha Atomic Research Centre, Mumbai 400 085, India

MS received 23 August 2014; accepted 5 November 2015

Abstract. **The $LiNi_{0.4}M_{0.1}Mn_{1.5}O_4$ (M = Co, Mg) solid solutions are synthesized by citric acid assisted sol–gel method and characterized by using TG/DTA, XRD, FTIR, EPR and SEM. The electrochemical characterization is carried out using CR-2032 coin type cell configuration. The cyclic voltammogram shows two pairs of redox current peaks, 4.35/3.80 V and 4.90/4.37 V *vs.* Li in a typical case of Co-doped sample, ascribed to two-step reversible intercalation of Li. A.c.-impedance (Nyquist plot) shows high frequency semicircle and a sloping line in the low-frequency region. The semicircle is ascribed to Li-ion migration through interface from the surface layer of the particles to electrolyte. The $LiNi_{0.4}Co_{0.1}Mn_{1.5}O_4$ shows reasonably good capacity retention in 20 cycles of galvanostatic charge/discharge cycling.**

Keywords. **Lithium ion batteries; positive electrode; $LiNi_{0.5}Mn_{1.5}O_4$-based spinels; sol–gel method; charge/discharge.**

1. Introduction

Lithium ion batteries (LIB's) are used in most of the mobile electronic devices and are being considered even for heavy electric vehicles and renewable energy power stations. A huge series of Li-storage cathode materials have been explored in the past two decades [1]. Among those, $LiMn_2O_4$ was found to be a potential substitute for $LiCoO_2$ in terms of cost, abundance and environmental compatibility [2–8]. However, the specific capacity of pure spinel decreases slowly after repeated cyclings at high temperature. It is well known that the decrease in capacity is due to number of factors, including Jahn–Teller distortion, dissolution of manganese into the electrolyte, lattice instability and particle size distribution [9–12]. To overcome these challenges, several divalent and trivalent doped ions such as Cr, Zn, Cu, Ga, Co, Al, Ni and Nb have been investigated [13–16].

It is well known that $LiMn_2O_4$ has a cubic spinel structure (*Fd3m*) with a unit cell constant of about 0.82 nm. Li and Mn resides in the 8a tetrahedral site and 16d octahedral site in lattice, respectively [17]. The $Mn^{3+/4+}$ state promotes the deinsertion process of Li^+ in $LiMn_2O_4$. This process is facilitated by the organic liquid electrolyte (1 : 1 volume of 1 M $LiPF_6$ in ethylene carbonate and dimethyl carbonate). In $LiM_xMn_{2-x}O_4$ lattice, the diffusion of Li^+ ion is associated with redox reaction of the substituted M cations because Mn^{4+} do not participate in the redox reactions between 2.7–4.7 V [18].

In recent times, it has been established that double doping in Mn^{3+} improves the cycling behaviour of the spinel-based cathodes [19]. Therefore, in this direction, we have focussed on double-doped $LiNi_{0.4}M_{0.1}Mn_{1.5}O_4$ (M = Co, Mg) materials by sol–gel method.

Especially, the traditional method to synthesize spinel $LiMn_2O_4$ is solid-state reaction, which is time-consuming, often requires extensive mechanical mixing, high sintering temperature and extended sintering process that are detrimental to the quality of the final product. Still, the usual method to synthesize spinel $LiMn_2O_4$ is solid-state reaction, which regularly leads to inhomogeneties, irregular morphology, broad distribution of particle sizes and also which is time-consuming, frequently requires extensive mechanical mixing, and high sintering temperature [20,21]. To conquer these drawbacks, we have adopted a sol–gel method using citric acid. The details on synthesis, structural, electrical and electrochemical behaviour are reported in this paper.

2. Experimental

2.1 *Sample preparation*

$LiNi_{0.4}M_{0.1}Mn_{1.5}O_4$ (M = Co, Mg) was prepared by taking the stoichiometric amounts of $LiOH{\cdot}H_2O$, $(C_2H_3O_2)_2Ni{\cdot}4H_2O$, $(C_2H_3O_2)_2Co{\cdot}4H_2O$, $(C_2H_3O_2)_2Mn{\cdot}4H_2O$, and $Mg(OH)_2$ dissolved in deionized water. Citric acid monohydrate ($C_6H_8O_7{\cdot}H_2O$),

*Author for correspondence (jmanjanna@rediffmail.com)

a chelating agent was added to this solution. The muddle was stirred continuously at 90°C till it formed a sticky liquid gel. Then, it was dried at 150°C for 2 h and ground to fine powder in agate mortar and heated at 350°C for 4 h to obtain an intermediate compound. It was further heated at 900°C for 22 h to form $LiNi_{0.4}M_{0.1}Mn_{1.5}O_4$ (M = Co, Mg).

2.2 *Characterization*

X-ray diffraction (XRD) pattern was obtained using CuKα radiation (λ = 1.542 Å) with a Ni-filter. Scanning electron microscopy (SEM) was used to evaluate the morphology of the sample. Fourier transform infrared (FTIR) spectra were obtained with KBr pellets. Electron paramagnetic resonance (EPR) spectra were recorded with a 100 kHz field modulation operating at 9.8 GHz frequency.

For electrical and electrochemical studies, CR-2032 coin type cells were assembled: for positive electrode composites, the spinel powder (80 wt%), S R carbon black (15 wt%) and polyvinylidene fluoride (PVDF) (5 wt%) were ground with a drop of NMP solvent to form uniform slurry. This slurry coated on Al-foil was dried in ambient condition and cut to spherical discs. A Li-foil was used as negative electrode as well as reference electrode. The electrodes were separated by a Celgard® 2400 (polypropylene) soaked in the electrolyte, 1 M solution of $LiPF_6$ in ethylene carbonate–dimethyl carbonate (EC/DMC, 1:1). These components are assembled to CR-2032 coin type cells in argon filled glove box.

A cyclic voltammogram was recorded using Autolab PGSTAT 302n. The working electrode in CR-2032 coin type cell is the active cathode material and Li-foil served as a reference as well as a counter electrode. A scan rate of 0.1 mV s^{-1} between 3.5–4.9 V *vs.* Li was set. For the same sample, a.c.-impedance data was obtained in the frequency range of 10 kHz–100 mHz using fra 2.0 software. Charge–discharge cycle tests were carried out using Arbin battery system between 3.5 and 4.9 V at C/10 rate.

3. Results and discussion

3.1 *Structural characterization of materials*

To find the proper temperature range for the reaction, thermogravimetric/differential thermal analysis (TG/DTA) was carried out. A curve obtained for an intermediate gel precursor (heated at 350°C) for M = Co and Mg is shown in figure 1. We see three weight loss regions for both the samples: room temperature–200°C, 200–300°C and 300–450°C. The first region is attributed to loss of adsorbed water, second region is attributed to the loss of crystalline water and third region is attributed to the decomposition of hydroxides and acetates leading to the formation of final product. The DTA curve shows exothermic peaks corresponding to decomposition of crystalline water, hydroxides and acetates. It is clear that the formation of $LiNi_{0.4}M_{0.1}Mn_{1.5}O_4$ (M = Co, Mg)

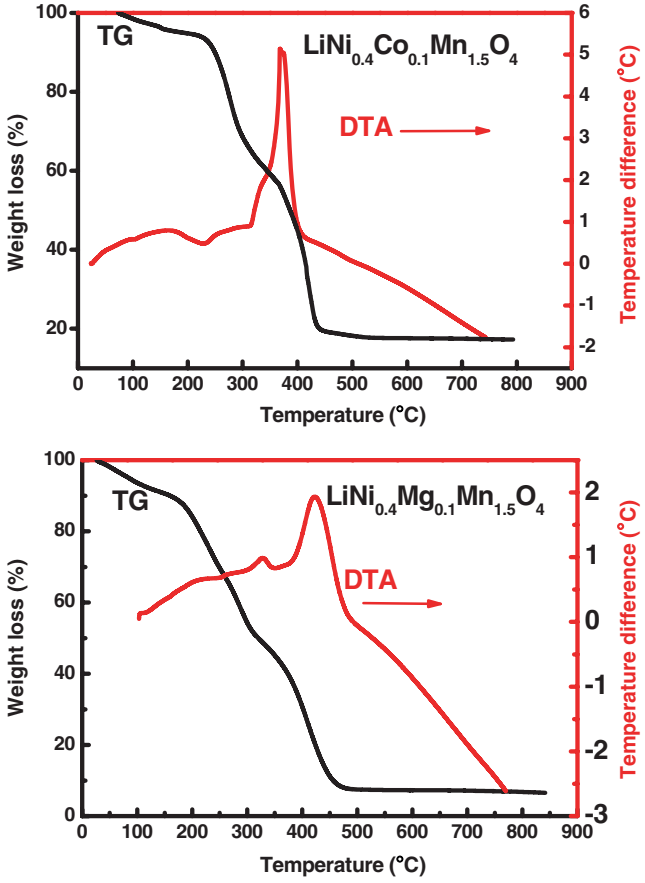

Figure 1. TG–DTA curves of $LiNi_{0.4}M_{0.1}Mn_{1.5}O_4$ (M = Co, Mg) precursors.

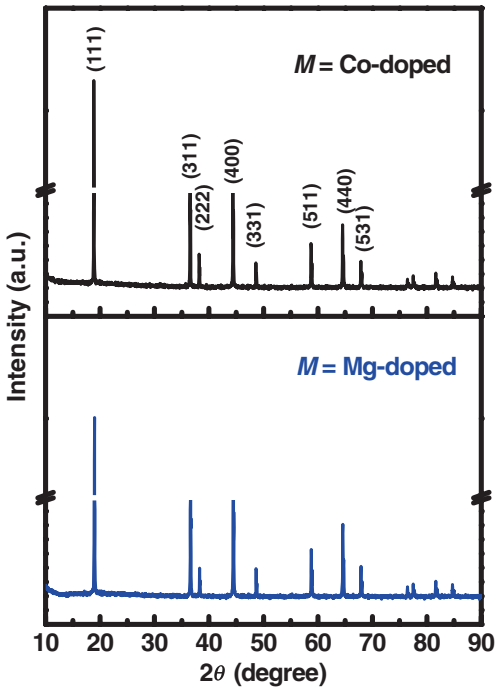

Figure 2. X-ray diffraction pattern of $LiNi_{0.4}M_{0.1}Mn_{1.5}O_4$ (M = Co, Mg).

occurs on heating to >450°C. Nevertheless, we have heated up to 900°C during the synthesis to ensure the formation of solid solutions.

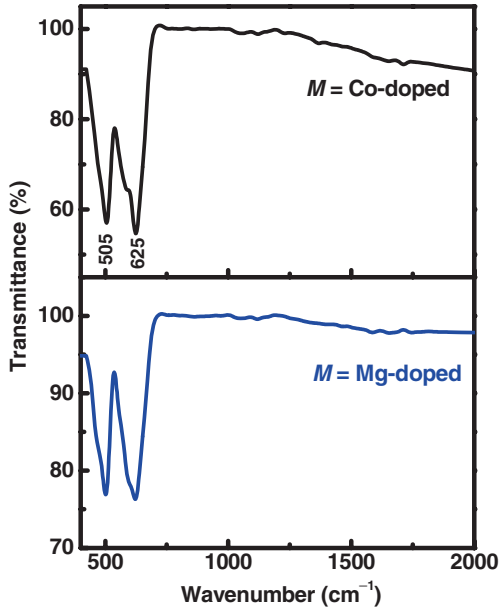

Figure 3. FTIR spectra of $LiNi_{0.4}M_{0.1}Mn_{1.5}O_4$ (M = Co, Mg).

The XRD patterns shown in figure 2 could be indexed in the *Fd3m* space group (JCPDS file no. 35-0782). The sharp XRD peaks indicate the well-crystalline cubic spinel structure. Accordingly, the Ni^{2+} and Mn^{4+} arbitrarily occupy the octahedral 16d sites, while the Li^+ ions occupy the tetrahedral 8a sites [22]. Based on the XRD peak broadening, the average crystallite size, d was calculated to be about 100 nm for all the samples using Scherer formula, $d = K\lambda/(\beta_1 \cos\theta)$. The FTIR studies on spinels have been undertaken by Yi *et al* [23] and Richardson *et al* [24]. In FTIR spectra (figure 3), the bands around 505 cm^{-1} and 625 cm^{-1} have been assigned to Li–O (of LiO_6 octahedra) and Li–Mn–O stretching vibrations (of MnO_6 octahedra), respectively [25–27]. SEM image of $LiNi_{0.4}M_{0.1}Mn_{1.5}O_4$ (M = Co, Mg) (figure 4) shows the polydispersed nature of particles and their agglomeration. The energy dispensive X-ray analysis (EDXA) shows all the constituent elements present in the expected levels (shown in table of figure 4) except Li which cannot be detected by EDXA.

3.2 *EPR studies*

The distribution of cation and changes in the Mn^{4+} environment during lithium extraction/insertion can be monitored by EPR spectroscopy. The sample, $LiNi_{0.4}Mg_{0.1}Mn_{1.5}O_4$ contains

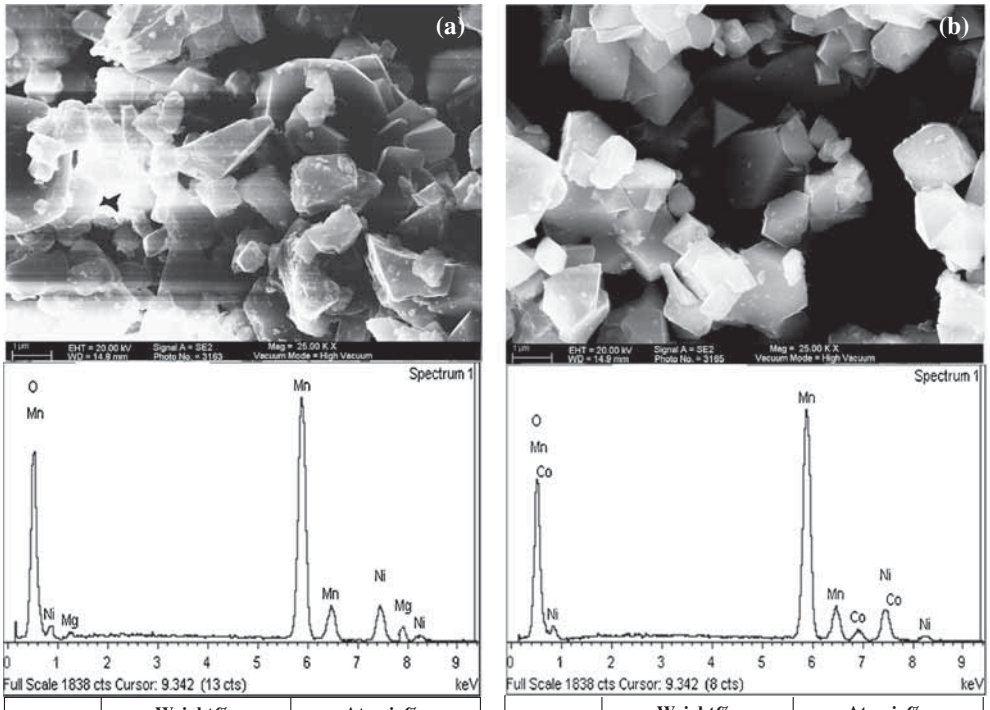

Element	Weight%		Atomic%	
	expected	obtained	expected	obtained
O K	37.14	26.40	66.66	65.72
Mn K	47.82	48.41	25	25.23
Mg K	1.41	1.02	1.66	1.34
Ni K	13.62	14.04	6.66	7.64
Total	100.00			

Element	Weight%		Atomic%	
	expected	obtained	expected	obtained
O K	36.42	36.63	66.66	65.83
Mn K	46.88	45.53	25	24.91
Co K	3.35	3.88	1.66	1.21
Ni K	13.35	13.86	6.66	6.92
Total	100.00			

Figure 4. SEM image (1 μm scale) of (**a**) $LiNi_{0.4}Mg_{0.1}Mn_{1.5}O_4$ and (**b**) $LiNi_{0.4}Co_{0.1}Mn_{1.5}O_4$.

two magnetic ions: Ni^{2+} (S = 1) and Mn^{4+} (S = 3/2). It is reported [28] that Ni^{2+} does not donate to the EPR spectrum because the deformation of crystal field and strains on the disparate sites spread out the resonance spectra and can no longer be detected. As shown in figure 5, the detected paramagnetic resonance for $LiNi_{0.4}Mg_{0.1}Mn_{1.5}O_4$ sample could only be attributed to the presence of octahedral Mn^{4+}. For $LiNi_{0.4}Co_{0.1}Mn_{1.5}O_4$, an additional magnetic ion due to Co^{2+} (S = 3/2) contributes to the overall magnetic moment. Thus, we see a relatively sharp EPR signal. The broad EPR signal in both the cases with Lorentzian shape centred at $g \approx 1.9$ dominates. It is an indicative of the ordered nature of the sample having paramagnetic interaction among 16d site ions in the spinel structure [29–31].

3.3 *Electrical and electrochemical characterization*

Nyquist plots of $LiNi_{0.4}M_{0.1}Mn_{1.5}O_4$ (M = Co, Mg) is recorded (figure 6) to study the kinetics of lithium de/insertion process, which were measured in the pristine state. It can be observed that the plot has a semicircle and a straight line. The charge–transfer resistance was found to be about 450 Ω (M = Mg) and 300 Ω (M = Co). These values indicate the formation of electrode/ electrolyte interface layer on the surface of cathode after charge–discharge cycling [32,33]. The impedance spectrum consists of a high frequency semi circle and a sloping line in low frequency ranges; high frequency range represents the migration of Li^+ ions at the electrode/electrolyte interface and the low frequency range corresponds to the charge–transfer process [34,35]. In fact, electrochemical impedance spectroscopy (EIS) could be considered as one of the most sensitive tools for the study of differences in the electrodes behaviour due to surface modification. To address porosity and inhomogeneities of electrodes, the double layer capacitance of electrode/electrolyte interface is replaced by a constant phase element (CPE). This CPE was used to obtain an equivalent circuit by substituting the double layer capacitance. The CPE is commonly used to describe the depressed semicircle that results from a porous electrode (inset of figure 6) [34,36–38]. According to the literature [39], the intercept at the Z' axis in the high frequency corresponds to ohmic resistance (R_s), which represents the resistance of the electrolyte. The sloping line in the

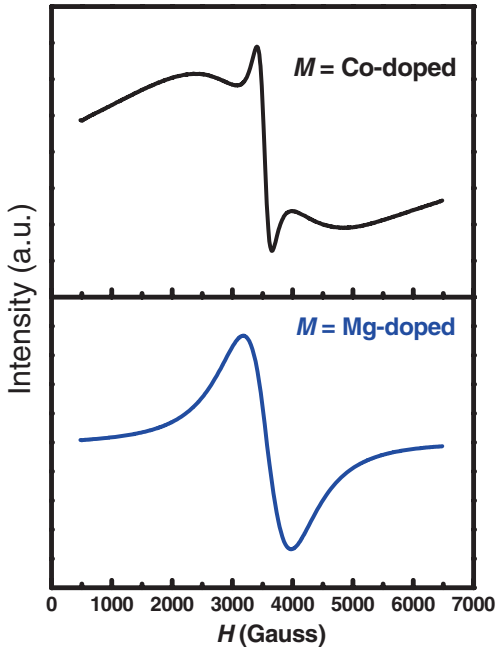

Figure 5. EPR spectrum of $LiNi_{0.4}M_{0.1}Mn_{1.5}O_4$ (M = Co, Mg).

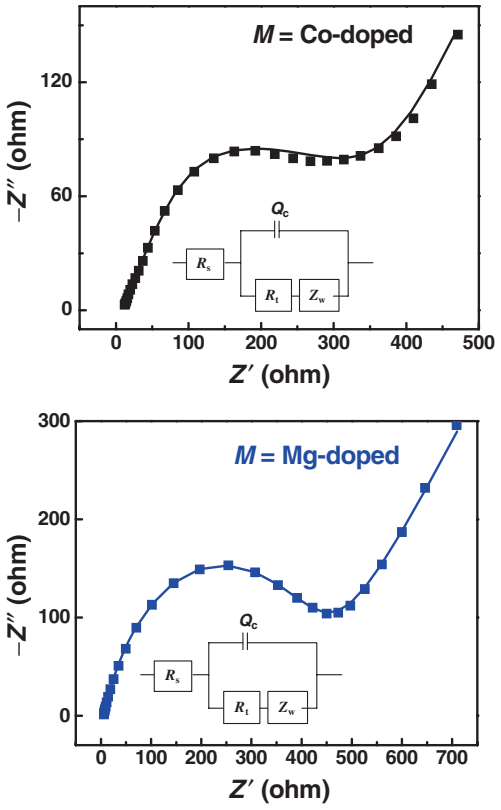

Figure 6. Nyquist plots of the $LiNi_{0.4}M_{0.1}Mn_{1.5}O_4$/half cell fitted to Randles equivalent circuit.

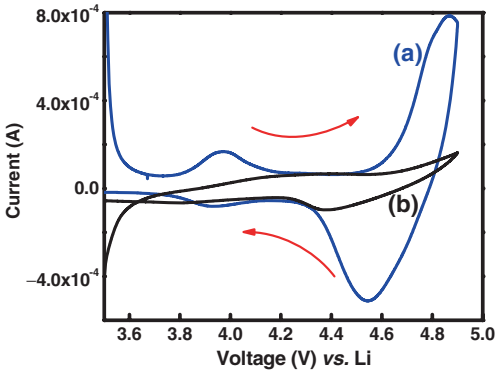

Figure 7. Cyclic voltammogram of **(a)** $LiNi_{0.4}Mg_{0.1}Mn_{1.5}O_4$ and **(b)** $LiNi_{0.4}Co_{0.1}Mn_{1.5}O_4$ at a scan rate of 0.1 mV s^{-1}.

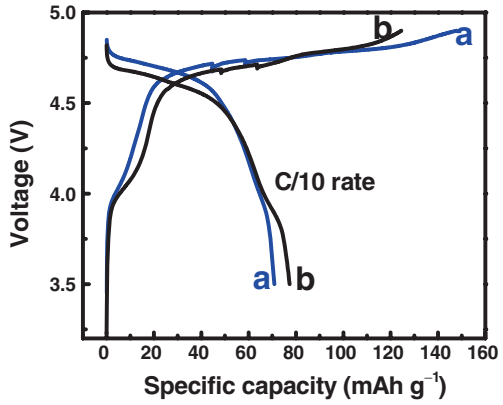

Figure 8. Galvanostatic voltage *vs.* capacity profile for a cell Li/$LiNi_{0.4}M_{0.1}Mn_{1.5}O_4$ (M = Co, Mg) at C/10.

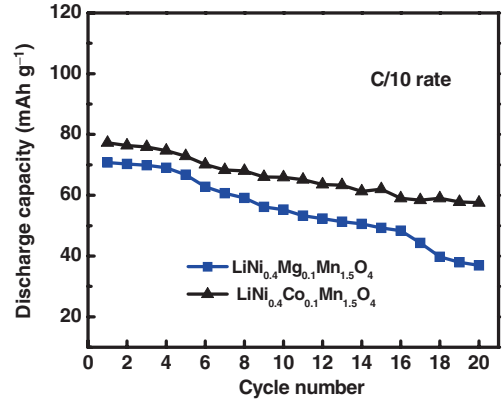

Figure 9. Discharge capacity *vs.* cycle number of $LiNi_{0.4}M_{0.1}Mn_{1.5}O_4$ (M = Co, Mg) at C/10 rate.

low frequency region indicates the charge transfer resistance (R_t) of the electrodes, Z_w is the Warburg impedance and Q_c is the constant-phase element. Constant phase element has been used to accommodate capacitor imperfections. The calculated values fitted well with the experimental values.

As shown in figure 7, two pairs of redox current peaks at 3.96/3.94 V and 4.86/4.54 V *vs.* Li for M = Mg and 4.35/3.80 and 4.90/4.37 V *vs.* Li for M = Co indicates that the Li^+ ions are de/inserted into the spinel $LiNi_{0.4}M_{0.1}Mn_{1.5}O_4$ lattice through a two-step process [40]. The redox performance observed here is in agreement with earlier reports [2,41].

Figure 8 shows the galvanostatic charge/discharge curves at a constant current rate of C/10 between 3.5 and 4.9 V. Figure 9 depicts the cycling performance of $LiNi_{0.4}M_{0.1}Mn_{1.5}O_4$ electrode for the 20 cycles at C/10 current rate. The specific discharge capacity for M = Co and Mg are 57 and 36 mAh g^{-1} at the end of 20 cycles, respectively. Thus, the performance of Co-doped sample is better than that of Mg-doped sample. The decrease in capacity here may be due to the large change in unit cell volume during the charge/discharge cycling [42]. In general, the specific capacity decrease at high current rates may be due to an increase in electrode polarization during cycling. In addition to slow down redox process of the cathode material, the electrode polarization can arise due to its inappropriateness with current collector and also the electrolyte [43]. In the present case, the capacity fading is more pronounced in the case of Mg-doped sample. This could be due to the relatively less stable lattice structure as ionic radius of Mg^{2+} (0.72 Å) is much bigger than that of Co^{2+} (0.58 Å) ≈ Mn^{3+} (0.65 Å). Such a difference in ionic size will impose lattice distortion on the solid solutions.

4. Conclusions

$LiNi_{0.4}M_{0.1}Mn_{1.5}O_4$ (M = Co, Mg) was successfully prepared by citric acid assisted sol–gel method. Cyclic voltammogram for these materials using coin-type cell shows two pairs of redox peaks corresponding to two-step reversible intercalation reaction. Among the compositions prepared here, $LiNi_{0.4}Co_{0.1}Mn_{1.5}O_4$ demonstrates reasonably good cycling performance in the voltage range of 3.5–4.9 V with capacity retention of 57 mAh g^{-1} at C/10 rate over the investigated 20 cycles. Nevertheless, the in-depth studies are needed to modify the sample characteristics to obtain the significant capacity retention and to adapt for 5 V applications.

Acknowledgement

One of the authors (G P Nayaka) gratefully acknowledges S Yallapaa, B M Vinoda and M Vinuth for their help during this research work and the Kuvempu University for financial support.

References

[1] Jeffrey W F 2010 *J. Power Sources* **195** 939
[2] Tarascan J M and Guyomard D 1991 *J. Electrochem. Soc.* **138** 2864
[3] Bellitto C, Bauer E M, Righini G, Green M A, Branford W R, Antonini A and Pasquali M 2004 *J. Phys. Chem. Solids* **65** 29
[4] Molenda J, Pałubiak D and Marzec J 2005 *J. Power Sources* **144** 176
[5] Lee A S, Kumada N and Yoshio M 2001 *J. Power Sources* **96** 376
[6] Robertson A D, Armstrong A R and Bruce P G 2001 *J. Power Sources* **97–98** 332
[7] Lee E S, Huq A and Manthiram A 2013 *J. Power Sources* **240** 193
[8] Liang Y Y, Bao S J and Li H L 2006 *J. Solid State Chem.* **179** 2133
[9] Zhong G B, Wang Y Y, Yu Y Q and Chen C H 2012 *J. Power Sources* **205** 385
[10] Amarilla J M, Petrov K, Pico F, Avdeev G, Rojo J M and Rojas R M 2009 *J. Power Sources* **191** 591
[11] Poizot P, Laruelle S, Grugeon S, Dupont L and Tarascon J M 2000 *Nature* **407** 496

[12] Xia Y Y, Yoshio M and Zhou Y H 1997 *J. Electrochem. Soc.* **144** 2593

[13] Ting F Y, Ying X, Yan R Z, Rong S Z and Ming F Y 2012 *J. Power Sources* **211** 59

[14] Mukerjee S, Yang X Q, Sun X, Lee S J, McBreen J and Eli Y E 2004 *Electrochim. Acta* **49** 3373

[15] Locati C, Lafont U, Simonin L, Ooms F and Kelder E M 2007 *J. Power Sources* **174** 847

[16] Jong H L, Jin K H, Dong H J, Sun Y K and Seung M O 2000 *J. Power Sources* **89** 7

[17] Masaka Y, Ralph J B and Akiya K (eds) 2010 *Lithium-ion batteries: science and technologies* (New York, USA: Springer, Cambridge University)

[18] Koyama Y, Yabuuchi N, Tanaka I, Adachi H and Ohzuku T 2004 *J. Electrochem. Soc.* **151** 499

[19] Thirunakaran R, Sivashanmugam A, Gopukumar S and Rajalakshmi R 2009 *J. Power Sources* **187** 565

[20] Rossen E, Reimers J R and Dahn J R 1993 *Solid State Ionics* **62** 53

[21] Alcantara R, Lavela P, Relano P L, Tirado J L, Zhecheva E and Stoyanova R 1998 *Inorg. Chem.* **37** 264

[22] Yang M C, Xu B, Cheng J H, Pan C J, Hwang B J and Meng Y S 2011 *Chem. Mater.* **23** 2832

[23] Yi T, Hu X and Gao K 2006 *J. Power Sources* **162** 636

[24] Richardson T J, Wen S J, Striebel K A, Ross P N and Cairns E J 1997 *Mater. Res. Bull.* **32** 609

[25] Richardson T J and Ross P N Jr 1996 *Mater. Res. Bull.* **31** 935

[26] Halan M, Berchmans L J and Hussain A Z 2010 *Ionics* **16** 227

[27] Nayaka G P, Manjanna J, Anjaneya K C, Manikandan P, Periasamy P and Tripathi V S 2014 *Bull. Mater. Sci.* **37** 711

[28] Mandal S, Rojas R M, Amarilla J M, Calle P, Kosova N V, Anufrienko V F and Rojo J M 2002 *Chem. Mater.* **14** 1598

[29] Stoyanova R, Gorova M and Zhecheva E 2000 *J. Phys. Chem. Solids* **61** 615

[30] Massarotti V, Capsoni D, Bini M, Azzoni C B and Paleari A 1997 *J. Solid State Chem.* **128** 80

[31] Stoyanova R K, Zhecheva E N and Gorova M Y 2000 *J. Mater. Chem.* **10** 1377

[32] Aurbach D, Levi M D, Levi E, Telier H, Markovsky B and Salitra G 1998 *J. Electrochem. Soc.* **145** 3024

[33] Sun Y K, Kim D W and Choi Y M 1999 *J. Power Sources* **79** 231

[34] Takahashi M, Tobishima S I, Takei K and Sakurai Y 2002 *Solid State Ionics* **148** 283

[35] Sung W O, Seung T M, Han B K and Yang K S 2009 *J. Power Sources* **189** 756

[36] Macdonald J R 1984 *Solid State Ionics* **13** 147

[37] Narayanan S R, Shen D H, Surampudi S, Attia A I and Hal-Pert G 1993 *J. Electrochem. Soc.* **140** 1854

[38] Funabiki A, Inaba M, Ogumi Z, Yuasa S, Otsuji J and Tasaka A 1998 *J. Electrochem. Soc.* **145** 172

[39] Li L M, Guo H J, Li X H, Wang Z X, Peng W J, Xiang K X and Cao X 2009 *J. Power Sources* **189** 45

[40] Ke D, Rong H G, Dong P Z and Lu Q 2010 *Electrochim. Acta* **55** 1733

[41] Yamane H, Inoue T, Fujita M and Sano M 2001 *J. Power Sources* **99** 60

[42] Ohzuku T and Ueda A 1994 *J. Electrochem. Soc.* **141** 2972

[43] Linden D 1995 *Handbook of batteries* (New York: McGraw-Hill)